

Millimeter Interferometer Observations of Flares

Stephen M. WHITE

Astronomy Department, University of Maryland, College Park, MD 20742, U.S.A.

E-mail: white@astro.umd.edu

Abstract

This paper addresses the current state of millimeter interferometry of solar flares and the issues which can be addressed by such observations. Millimeter interferometers such as BIMA detect gyrosynchrotron emission from MeV-energy electrons in the impulsive phase of solar flares as well as from hot dense plasma in the thermal decay phase. BIMA now consists of 10 antennas and is capable of snapshot imaging of solar flares with excellent spatial resolution and dynamic range of up to 100. The properties of MeV-energy electrons deduced from such observations vary widely: in some flares they are present for a much shorter time than the lower-energy hard-X-ray producing electrons, while in other flares they are present longer. Examples of both circumstances are given. It is widely observed that the energy distribution determined from the optically-thin radio spectrum is inconsistent with that determined from hard X-ray data: generally this is interpreted to mean that the electron energy distribution is flatter at higher energies, but even this interpretation can run into difficulties. This discrepancy between radio and hard X-ray spectral indices may be revealing something fundamental about electron acceleration in solar flares.

Key words: Sun: flares — Sun: radio radiation — Instrumentation: interferometers

1. Introduction

The general properties of millimeter emission from solar flares are now well-established: it is produced both in the impulsive phase and in the gradual decay phase of flares. The importance of millimeter-wavelength observations in the impulsive phase is that they are only sensitive to the most energetic electrons accelerated by solar flares, and not the electrons in the energy range below 500 keV which can dominate microwave emission. This fact results from the combination of the characteristics of the mechanism which produces the impulsive radio emission from solar flares (gyroresonance emission, i.e., radiation due to the acceleration of electrons spiraling in a magnetic field), and the range of magnetic field strengths typical of the corona. Gyroresonance emission takes place at harmonics of the local gyrofrequency, broadened by thermal motion. Typical coronal gyrofrequencies have an upper limit of order 5 GHz, so that any gyroemission at our observing frequency (~ 90 GHz, wavelength 3.5 mm) must be produced at gyroharmonics of at least 20, and usually higher. However, nonrelativistic electrons have effectively no opacity at such high harmonics: we know from the theory of gyroemission (i.e., synchrotron theory, in the high harmonic limit) that the typical harmonic radiated by a particle with energy γmc^2 is γ^3 . Thus emission at harmonics higher than 20 requires electrons with γ at least of order 3. Quantitative calculations verify the conclusion that only MeV-energy electrons can produce significant gyrosynchrotron emission at 3 mm wavelength (White & Kundu 1992). These electrons radiate so strongly that they make millimeter observations a much more sensitive diagnostic of MeV electrons than are γ -ray observations: we have demonstrated that even in small flares (down to C1 GOES soft X-ray class) the impulsive-phase emission is readily detected, and thus MeV electrons can be studied (Kundu et al. 1990; White et al. 1992; Lim et al. 1992; Kundu et al. 1994).

The principal scientific issue addressed by millimeter observations of flares is the acceleration of electrons to high energies in solar flares. It is well established that in the impulsive phase of solar flares, energy is converted from a form stored as magnetic field energy into particle kinetic energy. One aspect of this conversion is the production of the 20–200 keV electrons which produce the bulk of the observed hard X-rays, and GRO's detectors are sensitive enough to see hard X-rays in this energy range from virtually all flares. There is evidence from hard X-ray observations that typical flare energy spectra show a “break downwards” in this energy range, with the spectrum becoming steeper at high energies. On the other hand, observations of the radio spectrum out to millimeter wavelengths suggest the opposite result: namely, that there is a flattening of the electron energy spectrum at high energies (~ 1 MeV), required to explain the relatively large millimeter fluxes detected in observations with millimeter-wavelength

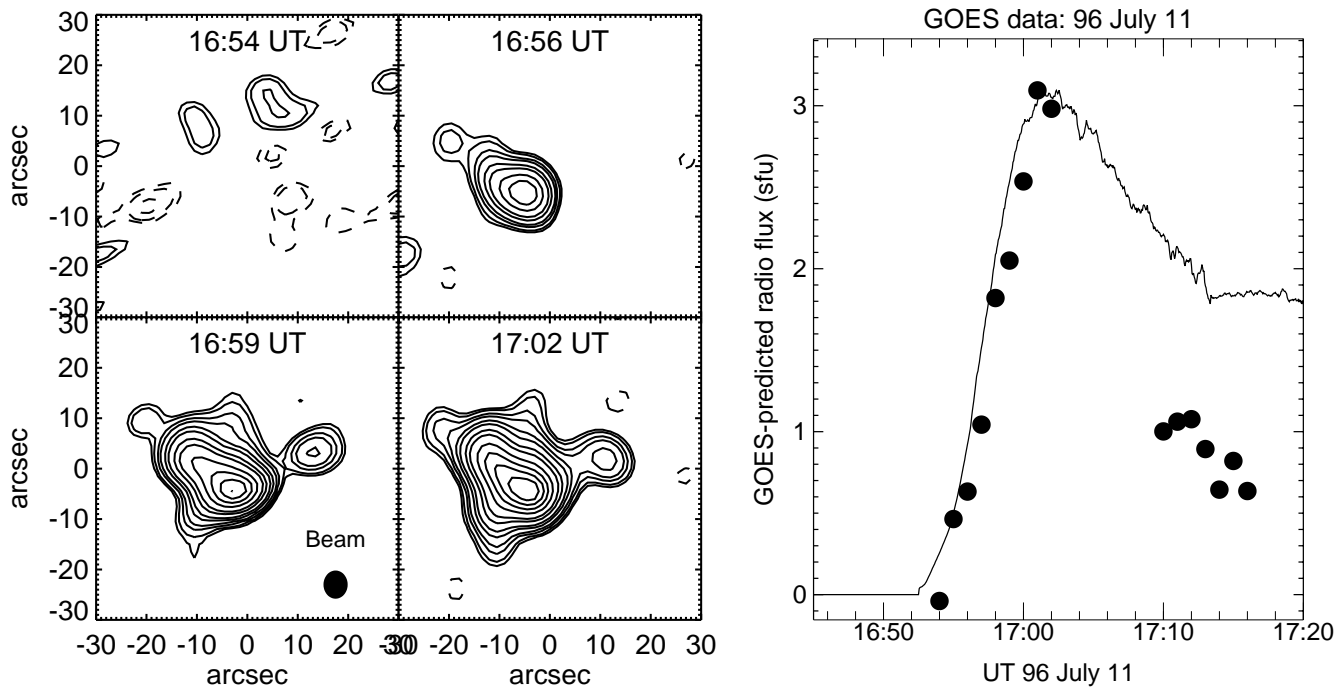


Fig. 1. BIMA observation (using 9 antennas) of a gradual flare on 1996 July 11. The images at left show the evolution of the radio source with time. The beam size is $7'' \times 6''$ (shown in the bottom left panel). The source is well resolved at this resolution. The panel on the right compares the behaviour of the radio flux at 86 GHz expected to be emitted from the soft-X-ray-emitting plasma detected by the GOES satellites (solid line) with the (scaled) CLEANed fluxes obtained from the images. This event is consistent with being a purely thermal event, with no nonthermal emission. The dynamic range of the 17:02 UT image is of order 100 (after self-calibration). Contours are plotted at multiples 3, 4, 6, 8, 12, 16, 24, 32, 48, 64, 80, and 96 of 2.5 Jy (negative contours are dashed).

telescopes. Occasionally such flattening is also seen in the hard X-ray spectra of very large flares (e.g., Dennis 1988, Trotter 1998). The combination of these two results suggests that there are several distinct electron populations produced in flares: the 20–200 keV population, which receives the bulk of the energy converted to electron kinetic energy; and a hard component which typically has a flatter spectrum.

We discuss these issues in the remainder of this paper with the aid of two examples. The next section, however, presents an example of the sort of flare data which can be acquired with BIMA, presently consisting of 10 antennas.

2. Current Capabilities of Millimeter Interferometry

Most millimeter interferometer observations of flares have been carried out with the Berkeley–Illinois–Maryland Array (BIMA) in northern California. This array has been evolving over the years (it is funded by the NSF and the university partners for primarily galactic and extragalactic studies, with a significant solar component), from a 3-element array during the first solar observations (Kundu et al. 1990) to a 6-element array which was used for the first true high-spatial-resolution interferometer images of a flare (Silva et al. 1996; Silva et al. 1997) and more recently a 9-element array and now a 10-element array. The significance of the number of antennas in the array is the improvement in the instantaneous spatial coverage of the telescope: the number of baselines, each corresponding to a different spatial scale on the sky, increases as the square of the number of antennas, so we are able to map much more complicated structures when we have more antennas.

Figure 1 demonstrates this for an event observed with 9 antennas in 1996. This particular event showed no evidence for non-thermal emission: as the right panel of Figure 1 shows, the behaviour of the radio flux observed by BIMA matches the expected thermal emission from the soft-X-ray-emitting plasma very well during the rise of the X-rays. It does not match as well during the decay, but that is to be expected if the source size expands so that it is larger than the largest spatial scale which the interferometer can measure. Note that the flux scales do not match

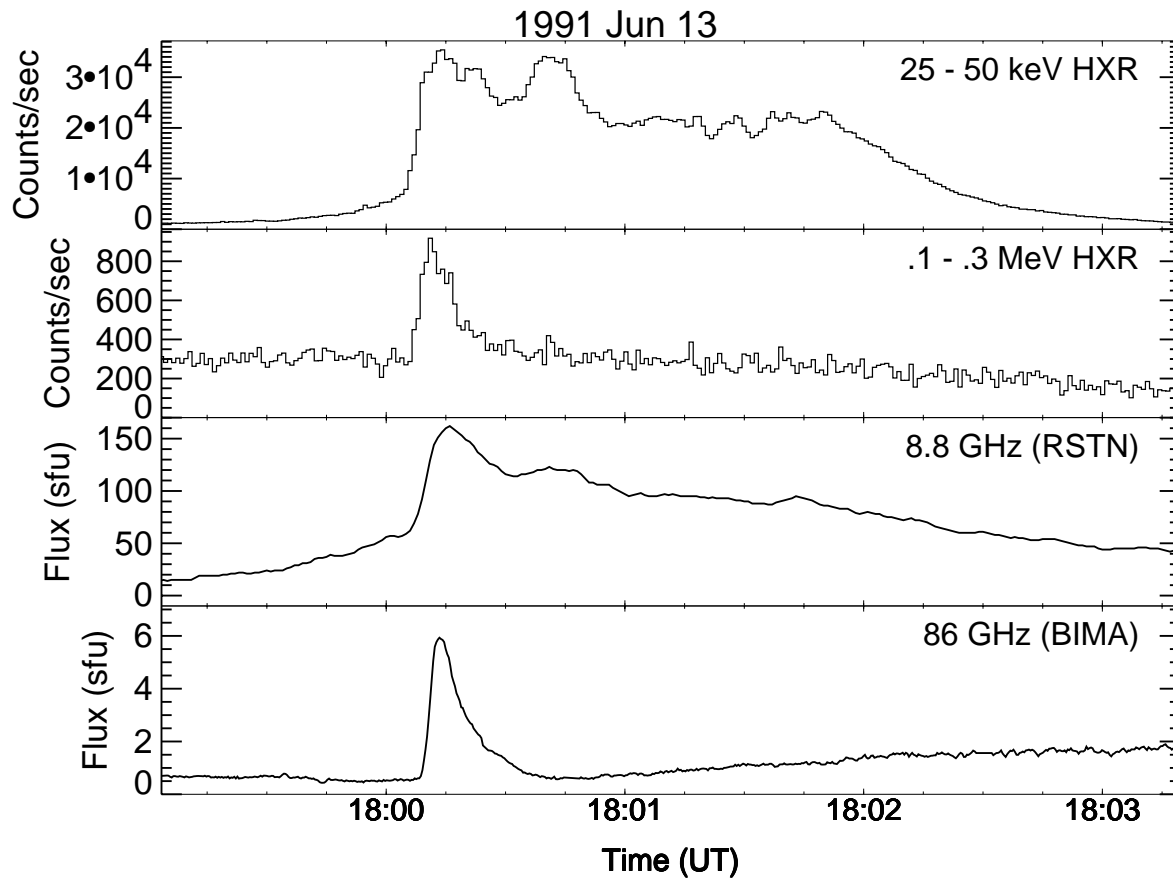


Fig. 2.. The time profile of a flare observed on 1991 June 13 in two hard X-ray energy ranges of the BATSE large-area detector (as labeled), at 8.8 GHz (RSTN data) and at 86 GHz (BIMA data). Note that the 25 – 50 keV emission continues much longer than do the higher-energy X-rays: the latter are confined to a hard spike at the onset of the flare. The time resolution of the BATSE data is 1.024 s.

exactly as shown: the BIMA amplitudes have been scaled by a factor of order 2 for presentation. Possible causes for this discrepancy are that the fit to the GOES data does not represent all the material present, the assumed $[\text{Fe}/\text{H}]$ abundance may be wrong or BIMA's calibration may be wrong. The gap in the BIMA fluxes from 17:03 – 17:09 resulted from a calibrator observation.

The images in Figure 1 were made by first carrying out a preflare subtraction of the visibilities and then mapping and self-calibrating the resulting data set (the shortest baseline was omitted from the data because the preflare flux was very large and preflare subtraction did not work very well on this baseline). At the peak of the flare the source is quite large and well-resolved by the $7'' \times 6''$ beam. The nominal signal-to-noise achieved was of order 100, which roughly matches that achieved during VLA microwave snapshot imaging of flares.

These images demonstrate the potential of millimeter interferometry for solar flare work. Presently BIMA has 10 antennas but with new receivers which require a special solar calibration scheme presently being developed. We expect that it will provide some excellent data during the coming solar maximum.

3. Event of 1991 June 13: Hard-Soft Evolution

In this section we present an event which demonstrates the general result that the MeV-energy electrons seem to be a population quite different from the accelerated electrons which produce hard X-rays (White et al. 1998). Figure 2 presents light curves in two hard X-ray energy ranges, one microwave frequency on the optically-thick side of the radio spectrum, and millimeter data on the optically-thin side of the radio spectrum. This particular event has several interesting features: X-rays are only detected in the harder channel during a spike in the impulsive rise

phase of the event. Thereafter the hard X-ray flux in the lower energy range remains at the same level for almost 2 minutes, while the high-energy photons vanish after about 15 seconds. Spectral analysis of the X-ray data shows a sharp softening of the spectrum in accord with the light curves. The photon spectral index is about 4.5 during the initial hard spike but drops to about 6 later in the event.

The 8.8 GHz microwave data show a profile which is quite similar to the lower-energy hard X-rays, albeit with a slightly more pronounced spike at onset. The 86 GHz time profile, on the other hand, is clearly more similar to the 100 – 300 keV hard X-ray profile, with emission only during a brief spike at onset (emission consistent with thermal bremsstrahlung from the soft-X-ray-emitting plasma is also seen later in the event). This event thus suggests that MeV-energy electrons are only present during the onset of the event, whereas lower-energy 25 keV-X-ray-emitting electrons are present for a much longer time. Such behaviour is not consistent with, for example, the collisional evolution of a single population of electrons injected at flare onset: collisional evolution removes the lower-energy electrons first, since they have higher collision rates. Thus the character of electron acceleration apparently changed during the course of the event.

In this event, we do not have the data to determine whether the millimeter data are consistent with the hard X-ray spectrum during the hard spike at the onset of the flare: the radio spectrum had a very high turnover frequency and we do not have any other frequency clearly known to be above the spectral peak apart from the millimeter data. Taking the BIMA flux, extrapolating it lower in frequency according to the energy distribution of the hard X-ray-emitting electrons and comparing the result with the measured 15 GHz flux, we can say that the turnover frequency had to be well over 20 GHz, which is unusual.

The next event is one in which the addition of imaging data at millimeter wavelengths allows much tighter constraints to be placed on the electron populations present.

4. Event of 1994 August 16: Soft–Hard Evolution

This event occurred in AR 7765 on August 16, 1994, at 23 UT and was classified as a GOES B5.6 X-ray flare with peak emission at 23:12 UT. We have NRH, BIMA and OVRO radio data and CGRO/BATSE hard X-ray data for this event, and Yohkoh/SXT soft X-ray images during the decay phase but not the impulsive phase (Raulin et al. 1998). The remarkable aspect of this flare is evidence for the presence of MeV-energy electrons, which are responsible for the nonthermal millimeter emission, at a time when no hard X-rays from lower-energy electrons are detected. Figure 3 presents light curves in hard X-rays and at several radio frequencies from 3 to 86 GHz. The puzzling period of nonthermal millimeter emission in the absence of detectable hard X-ray emission occurs during a smoothly varying phase (23:04:20 – 23:07:00) which is seen at radio wavelengths to last several minutes and is the brightest phase at millimeter wavelengths, but is undetected in hard X-rays: it follows a brief spike of emission at flare onset which has the more usual properties of impulsive events and features nonthermal microwave, millimeter and hard X-ray emission.

We interpret the phase which is brightest at millimeter wavelengths as due to efficient trapping of a relatively small number of nonthermal electrons, whereas during the hard X-ray emission trapping is much less efficient and the decay time is much shorter at all energies, leading to a larger ratio of hard X-ray flux to radio flux. There does need to be a separate injection of electrons to explain the millimeter phase, since the number of MeV-energy electrons present in the corona clearly must be increasing from 23:04 to 23:05 UT in order for the optically-thin radio flux at 17 and 86 GHz to be increasing during this time, and this increase cannot be achieved simply by a change in the energy distribution such as removing the low-energy electrons. “Second-step” acceleration, as is invoked by Frost & Dennis (1971) for a similar-looking event in hard X-rays, is a possible explanation but requires that the seed electrons accelerated in the impulsive phase be trapped somewhere in the corona from where they cannot escape (since the HXR bremsstrahlung ceases at 23:04 UT) until the second acceleration mechanism kicks in and accelerates them subsequently when the millimeter emission is observed. Further, since the millimeter emission during the hard X-ray phase decays as rapidly as the hard X-rays and microwaves, the trapping time in the hard X-ray phase of the event must be short for all energies. This again is not consistent with collisional scattering, which causes lower-energy electrons to have much shorter trapping times than MeV-energy electrons.

As in many previous events studied at millimeter wavelengths, there is a discrepancy between the electron energy spectral indices inferred from the millimeter and hard X-ray data during the impulsive phase when both are detected: again it appears that the energy spectrum at 1 MeV must be significantly flatter than at several hundred keV and below. Based on the thick-target assumption for the hard X-rays, the electrons emitting the hard X-rays have an $E^{-4.9}$ energy distribution, while the radio-emitting electrons have an $E^{-3.6}$ distribution. As has been usual in the past, we could simply assume that the radio-emitting electrons are a higher-energy component with a flatter

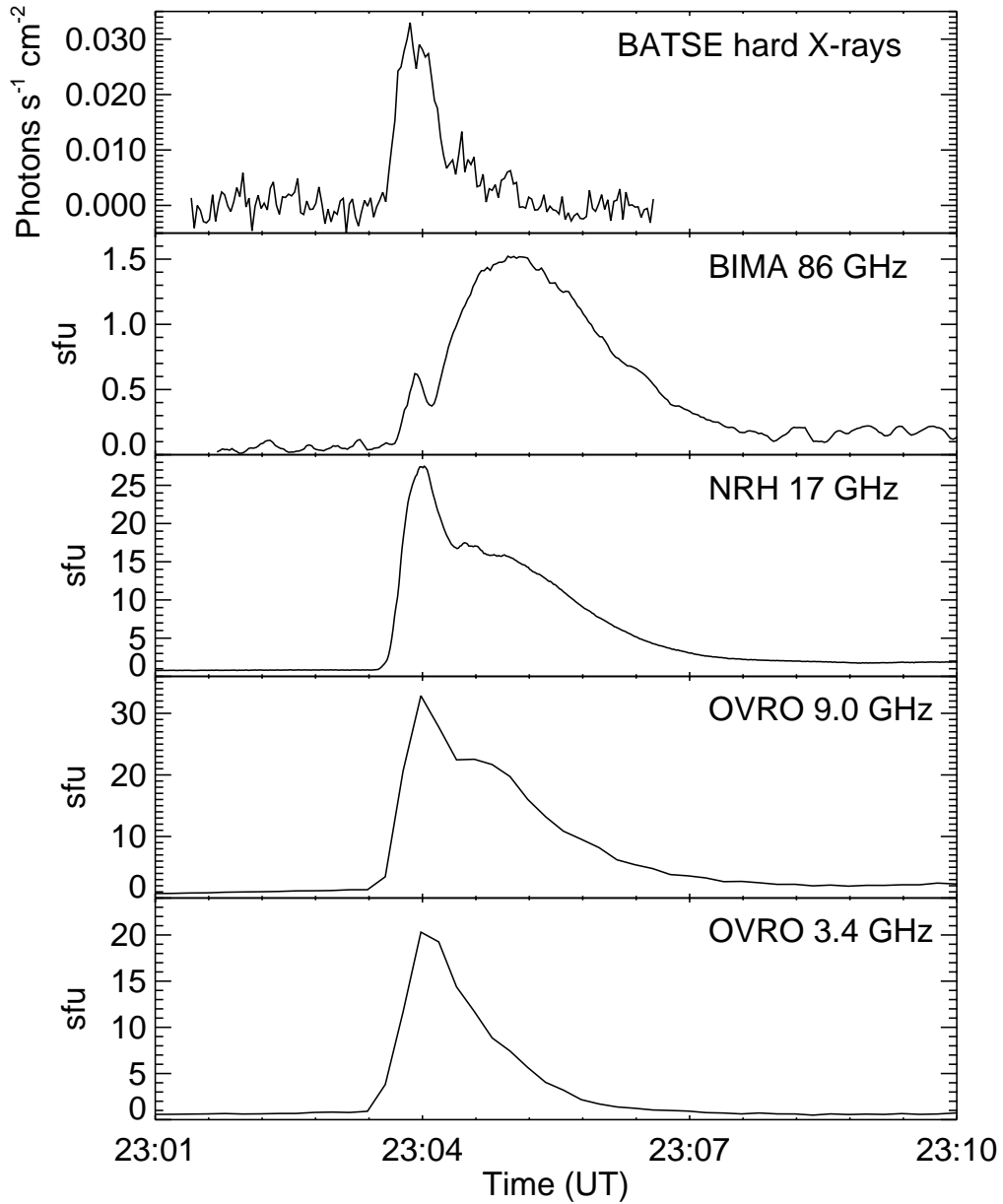


Fig. 3. Comparison of time profiles observed by BATSE, OVRO, BIMA and NRH during the impulsive phase and initial part of the gradual phase of the flare on 1994 August 16. The top panel shows the BATSE hard X-ray light curve. The second panel shows the BIMA 86 GHz flux measured on the longest baseline, in order to highlight the brief impulsive spike at 23:04 UT; note that the peak flux on shorter baselines is larger than shown here. The third panel shows 17 GHz data from NRH. These data are the “correlation coefficient” data which measure the flux in compact sources, scaled to match the flux in maps made at discrete times during the event from which the absolute flux can be determined. The three lower panels show the correlated flux between the two 27 m antennas at OVRO at 9.0 (3rd panel), 7.0 (4th panel) and 3.4 GHz (bottom panel), at 12 second time resolution.

spectrum than the hard X-ray emitting electrons. However, the fact that we can image the millimeter source in this case imposes constraints on the parameters of the radiating electrons. During the hard X-ray emission, BIMA measures an 86 GHz source size of order $13'' \times 7''$. For a magnetic field of 300 G in the radio source, which is consistent both with a photospheric magnetogram and with the location of the radio spectral peak, the number of electrons required to explain the observed radio fluxes exceeds at 50 keV the number of electrons required to explain the hard X-ray flux from a loop of the observed dimension. In other words, hard X-rays from the radio-emitting electrons should dominate the hard X-ray spectrum, and should produce a photon spectral index consistent with the radio spectrum. If the parameters of the source were not known, we could not constrain the electron numbers in this fashion, demonstrating the power of the imaging data. The discrepancy between the two populations can be ameliorated by assuming a much larger magnetic field than is plausible based on the photospheric fields, but it does not vanish (Raulin et al. 1998).

5. Discussion

This paper has emphasized the ways in which millimeter observations of flares can be used in conjunction with microwave and hard X-ray data to examine the different electron populations accelerated in solar flares. The millimeter data clearly imply that the higher-energy electrons which radiate at millimeter wavelengths belong to a population different from the nonthermal electrons which radiate at hard X-ray energies.

In particular, radio data almost always imply a harder energy spectrum than do hard X-ray data (e.g., Alissandrakis 1986; Staehli, Gary & Hurford 1989; Nitta et al. 1991; Lim et al. 1992; Kundu et al. 1994; Silva et al. 1996; Silva et al. 1997). Usually we dismiss this as due to a break upwards in the energy distribution at some point, although most X-ray astronomers assume a break down at around 100 keV (Lin & Schwartz 1987; Dulk, Kiplinger & Winglee 1992). However, such a broken-up spectrum may not always be truly quantitatively consistent with the data, as in the 1994 August 16 event, and it is possible that such an interpretation is overlooking something important about the emission of solar flares. High-quality multi-wavelength (hard X-ray, soft X-ray, microwave and millimeter) spatially-resolved observations are required to address this issue.

This work has been supported by NSF grant ATM-96-12738 and NASA grant NAG-W-1541. This research has made use of data obtained through the CGRO BATSE Solar Flare Data Archive maintained by the Solar Data Analysis Center at NASA-Goddard Space Flight Center and provided by the BATSE team headed by Dr. Gerald Fishman. The soft x-ray images are from the Yohkoh mission of ISAS, Japan. The soft x-ray telescope was prepared by the Lockheed Palo Alto Research Laboratory, the National Astronomical Observatory of Japan, and the University of Tokyo with the support of NASA and ISAS. I thank the referee for comments which improved the paper.

References

- Alissandrakis, C. E. 1986, *Solar Phys.*, 104, 207.
 Dennis, B. R. 1988, *Solar Phys.*, 118, 49.
 Dulk, G. A., Kiplinger, A. L., & Winglee, R. M. 1992, *ApJ*, 389, 756.
 Frost, K. J., & Dennis, B. R. 1971, *ApJ*, 165, 655.
 Kundu, M. R., White, S. M., Gopalswamy, N., Bieging, J. H., & Hurford, G. J. 1990, *ApJL*, 358, L69.
 Kundu, M. R., White, S. M., Gopalswamy, N., & Lim, J. 1994, *ApJS*, 90, 599.
 Lim, J., White, S. M., Kundu, M. R., & Gary, D. E. 1992, *Solar Phys.*, 140, 343.
 Lin, R. P., & Schwartz, R. A. 1987, *ApJ*, 312, 462.
 Nitta, N., White, S. M., Schmahl, E. J., & Kundu, M. R. 1991, *Solar Phys.*, 132, 125.
 Raulin, J., White, S. M., Kundu, M. R., Silva, A. R., & Shibasaki, K. 1998, *ApJ*, submitted.
 Silva, A. V. L., Gary, D. E., White, S. M., Lin, R. P., & de Pater, I. 1997, *Solar Phys.*, 175, 157.
 Silva, A. V. L., White, S. M., Lin, R. P., de Pater, I., Shibasaki, K., Hudson, H. S., & Kundu, M. R. 1996, *ApJL*, 458, L49.
 Staehli, M., Gary, D. E., & Hurford, G. J. 1989, *Solar Phys.*, 120, 351.
 Trotter, G., Vilmer, N., Barat, C., Benz, A., Magun, A., Kuznetsov, A., Sunyaev, R., & Terekhov, O. 1998, *A&A*, 334, 1099.
 White, S. M., & Kundu, M. R. 1992, *Solar Phys.*, 141, 347.
 White, S. M., Kundu, M. R., Bastian, T. S., Gary, D. E., Hurford, G. J., Kucera, T., & Bieging, J. H. 1992, *ApJ*, 384, 656.
 White, S. M., Schwartz, R. A., Murphy, R., Kundu, M. R., & Gopalswamy, N. 1998, *ApJ*, in preparation.